



HAL
open science

S-Ethyl-Isothiocitrullin-Based Dipeptides and 1,2,4-Oxadiazole Pseudo-Dipeptides: Solid Phase Synthesis and Evaluation as NO Synthase Inhibitors

Elodie Mauchauffée, Jérémy Leroy, Jihanne Chamcham, Abdelaziz Ejjoumany, Manon Maurel, Lionel Nauton, Booma Ramassamy, Karima Mezghenna, Jean-Luc Boucher, Anne-Dominique Lajoix, et al.

► To cite this version:

Elodie Mauchauffée, Jérémy Leroy, Jihanne Chamcham, Abdelaziz Ejjoumany, Manon Maurel, et al. S-Ethyl-Isothiocitrullin-Based Dipeptides and 1,2,4-Oxadiazole Pseudo-Dipeptides: Solid Phase Synthesis and Evaluation as NO Synthase Inhibitors. *Molecules*, 2023, 28, pp.5085. 10.3390/molecules28135085 . hal-04145268

HAL Id: hal-04145268

<https://hal.science/hal-04145268v1>



Submitted on 29 Jun 2023

HAL is a multi-disciplinary open access archive for the deposit and dissemination of scientific research documents, whether they are published or not. The documents may come from teaching and research institutions in France or abroad, or from public or private research centers.

L'archive ouverte pluridisciplinaire **HAL**, est destinée au dépôt et à la diffusion de documents scientifiques de niveau recherche, publiés ou non, émanant des établissements d'enseignement et de recherche français ou étrangers, des laboratoires publics ou privés.

Article

S-Ethyl-Isothiocitrullin-Based Dipeptides and 1,2,4-Oxadiazole Pseudo-Dipeptides: Solid Phase Synthesis and Evaluation as NO Synthase Inhibitors

Elodie Mauchauffée¹, Jérémy Leroy², Jihanne Chamcham¹, Abdelaziz Ejjoumany¹, Manon Maurel^{1,†}, Lionel Nauton³, Booma Ramassamy⁴, Karima Mezghenna², Jean-Luc Boucher⁴, Anne-Dominique Lajoix^{2,*} and Jean-François Hernandez^{1,*}

¹ Institut des Biomolécules Max Mousseron, CNRS, Univ. Montpellier, ENSCM, Pôle Chimie Balard, 34293 Montpellier, France

² Centre Biocommunication en Cardio-Métabolique, Univ. Montpellier, UFR Pharmacie, 34093 Montpellier, France

³ Institut de Chimie de Clermont-Ferrand, Université Clermont-Auvergne, CNRS, 63178 Aubière, France

⁴ Laboratoire de Chimie et Biochimie Pharmacologiques et Toxicologiques, UMR 8601, CNRS, Université Paris Descartes, CEDEX 06, 75270 Paris, France

* Correspondence: anne-dominique.lajoix@umontpellier.fr (A.-D.L.); jean-francois.hernandez@umontpellier.fr (J.-F.H.)

† Current address: SpiroChem, Rosental Area, Mattenstrasse 22, 4058 Basel, Switzerland.

Abstract: We previously reported dipeptidomimetic compounds as inhibitors of neuronal and/or inducible NO synthases (n/iNOS) with significant selectivity against endothelial NOS (eNOS). They were composed of an S-ethylisothiocitrullin-like moiety linked to an extension through a peptide bond or a 1,2,4-oxadiazole link. Here, we developed two further series where the extension size was increased to establish more favorable interactions in the NOS substrate access channel. The extension was introduced on the solid phase by the reductive alkylation of an amino-piperidine moiety or an aminoethyl segment in the case of dipeptide-like and 1,2,4-oxadiazole compounds, respectively, with various benzaldehydes. Compared to the previous series, more potent inhibitors were identified with IC₅₀ in the micromolar to the submicromolar range, with significant selectivity toward nNOS. As expected, most compounds did not inhibit eNOS, and molecular modeling was carried out to characterize the reasons for the selectivity toward nNOS over eNOS. Spectral studies showed that compounds were interacting at the heme active site. Finally, selected inhibitors were found to inhibit intra-cellular iNOS and nNOS expressed in RAW264.7 and INS-1 cells, respectively.

Keywords: NO synthases; enzyme inhibitors; pseudo-dipeptides; isothiocitrulline; 1,2,4-oxadiazole; solid phase synthesis



Citation: Mauchauffée, E.; Leroy, J.; Chamcham, J.; Ejjoumany, A.; Maurel, M.; Nauton, L.; Ramassamy, B.; Mezghenna, K.; Boucher, J.-L.; Lajoix, A.-D.; et al. S-Ethyl-Isothiocitrullin-Based Dipeptides and 1,2,4-Oxadiazole Pseudo-Dipeptides: Solid Phase Synthesis and Evaluation as NO Synthase Inhibitors. *Molecules* **2023**, *28*, 5085. <https://doi.org/10.3390/molecules28135085>

Academic Editors: Letizia Crocetti and Maris Cinelli

Received: 2 June 2023

Revised: 23 June 2023

Accepted: 27 June 2023

Published: 29 June 2023



Copyright: © 2023 by the authors. Licensee MDPI, Basel, Switzerland. This article is an open access article distributed under the terms and conditions of the Creative Commons Attribution (CC BY) license (<https://creativecommons.org/licenses/by/4.0/>).

1. Introduction

Nitric oxide (NO) is a widespread cellular signaling molecule involved in a wide range of physiological functions, which depend on its production localization [1,2]. Indeed, in mammals, NO is produced from L-Arginine (L-Arg) by three enzyme isoforms called nitric oxide synthases (NOS), which first differ by their localization and mode of regulation [3]. Two are constitutively expressed and are activated by increased intracellular calcium, leading to the production of low levels of NO (i.e., nanomolar), which will mainly activate the soluble guanylate cyclase. (i) The neuronal NOS (nNOS) is mainly present in the brain where NO acts as a neurotransmitter but also in pancreatic β -cells to control insulin secretion [4,5]. (ii) The endothelial NOS (eNOS) is present in the vessel endothelium and mainly contributes to smooth muscle relaxation, impacting blood pressure. The third NOS is the inducible NOS (iNOS). It is expressed by macrophages in response to various pro-inflammatory cytokines and is intrinsically active (i.e., no need for elevated calcium

concentration), producing high NO levels (i.e., micromolar), which lead to the formation of toxic species, such as peroxynitrite or other radical species [6], making iNOS expression an important host defense mechanism [7]. Both NOS isoforms share the same structure organization with two domains separated by a calmodulin-binding sequence. (i) The *N*-terminal oxygenase domain contains the heme prosthetic group, a tetrahydrobiopterine co-factor and the substrate binding site, which is connected to the protein surface through the substrate access channel; (ii) the *C*-terminal reductase domain contains two flavine cofactors: FAD and FMN [3,8,9].

Overproduction of NO by nNOS and iNOS is associated with various pathophysiological states [2,10–13]. Overstimulation of nNOS is mainly involved in ischemia reperfusion injury following stroke [14,15] and is also shown to contribute to melanoma progression and metastasis [16]. In contrast, uncontrolled iNOS production is observed in numerous diseases, including sepsis, inflammation (e.g., rheumatoid arthritis), insulin resistance, some cancers, and asthma [5,17–22]. Thus, a potential therapeutical strategy is to develop NOS inhibitors [23], but one clinically useful inhibitor should be selective of the targeted isoform to spare the essential physiological roles of the two others. It is particularly true for eNOS, whose unwanted inhibition exposed to serious side effects. Unfortunately, obtaining such selectivity is a challenge because the substrate binding sites of the three isoforms are highly conserved [24–27]. Anyway, thanks to minor structural differences or discriminating inhibition mechanisms, selective inhibitors have been identified. For instance, Silverman's team exploited one residue difference between nNOS and eNOS to discover highly selective nNOS inhibitors [28–31]. Several types of selective iNOS inhibitors have been identified, including (i) amidine-type substrate analogs, such as NIL or W1400, which irreversibly inactivate iNOS only [32–34]; (ii) dimerization iNOS inhibitors [35,36]; and (iii) competitive and reversible inhibitors exploiting a variable second shell residue in the substrate access channel [37]. Unfortunately, whereas several iNOS inhibitors have been the object of clinical studies, none were found to be useful because of toxicity, bioavailability, or inefficiency issues [38–41]. While adverse outcomes might originate from insufficient selectivity toward eNOS or, more generally, the difficulty to spare NO beneficial effects in chronic treatments [23], the usefulness of iNOS inhibition is questioned [42]. However, NOS inhibition could be useful in acute conditions, such as stroke [42] and/or in a synergistic association with another drug [43–45]. Finally, although potent, reversible and highly selective nNOS inhibitors with potential interests in stroke and other neuronal disorders have been identified, attaining sufficient permeability across the blood–brain barrier still requires some effort [46,47].

In this context, we develop substrate-based dipeptidomimetic inhibitors following Silverman's strategy [28]. We initially attached an extension onto the carboxyl side of a non-selective substrate-based inhibitor such as thiocitrulline (Tci), *S*-alkyl-isothiocitrullines (*S*-Me- and *S*-Et-Itc), and *N*-alkyl-arginines (*N*-Me- and *N*-Et-Arg) [48]. The extension is expected to interact in the less conserved substrate access channel of the protein, thus potentially affording affinity and selectivity. This approach is supported by an original solid-phase synthetic strategy [49], which allows the convenient synthesis of a large number of compounds from a single supported precursor. In this study, we prepared libraries of thiocitrullines, *S*-alkyl-isothiocitrullines, and *N*-alkyl-arginines extended on their carboxylate group via an amide bond (dipeptide-like) or by replacing the amide bond with isosteric heterocycles (i.e., 1,2,4- and 1,3,4-oxadiazoles, 1,2,4-triazoles) [48]. Although no highly potent NOS inhibitor has been identified in this first study, inhibition data generally showed significant selectivity toward eNOS, as most compounds did not inhibit this isoform, and most were in favor of nNOS. By comparing the inhibition efficiency for each of the five substrate-based inhibitors and each type of linker, we found that the best inhibitors generally contained an *S*-ethyl-isothioureia moiety and either an amide bond or a 1,2,4-oxadiazole heterocycle as a linker (see JMV4246 and JMV3457 as examples in Figure 1). Among favorable extensions, we identified aminoalkyl moieties as observed in

previous reports [50,51]. Indeed, it was proposed that a basic amine group would establish an important ionic or hydrogen bond within the substrate access channel [28].

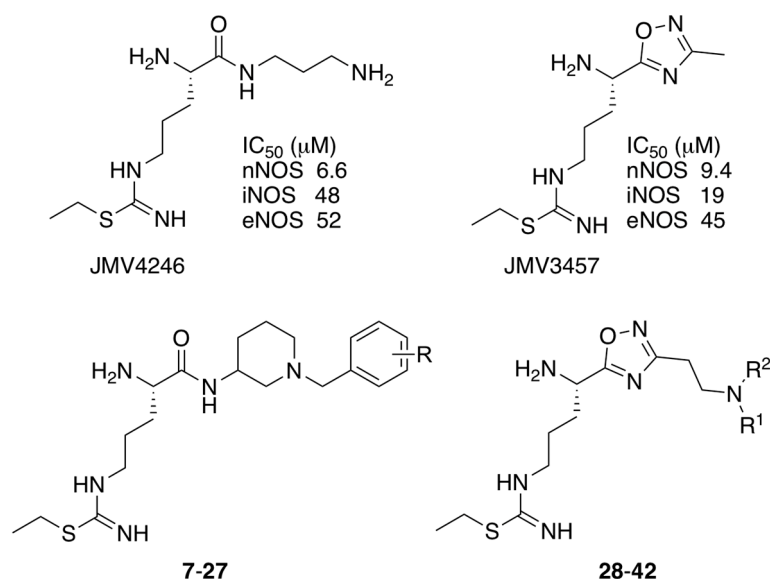


Figure 1. The structure of JMVs4246 and 3457 and the general structure of present series of dipeptides 7–27 and 1,2,4-oxadiazoles 28–42 ($R^1 = \text{H}$ or $\text{CH}_2\text{-Ar}$; $R^2 = \text{H}$ or R^1).

Based on these results, we kept these structural elements and further diversified the extension moiety. In particular, compared to our previously described compounds [48], we increased the length and/or volume of the extension to reach other regions of the substrate access channel where divergent interactions may take place, leading to higher potency and/or selectivity. We considered introducing variously substituted benzyl groups via reductive amination as a straightforward means to generate an extended series of compounds. The various substitutions on the benzene rings were chosen to obtain a diversity of chemical groups at different positions to try to establish beneficial interactions with the enzymes.

We presented a dipeptide-like series (compounds 7–27) containing diverse benzyl groups attached to piperidine and several series of 1,2,4-oxadiazole compounds (28–42) containing mono- or dibenzylated aminoethyl substituents (Figure 1).

2. Results and Discussion

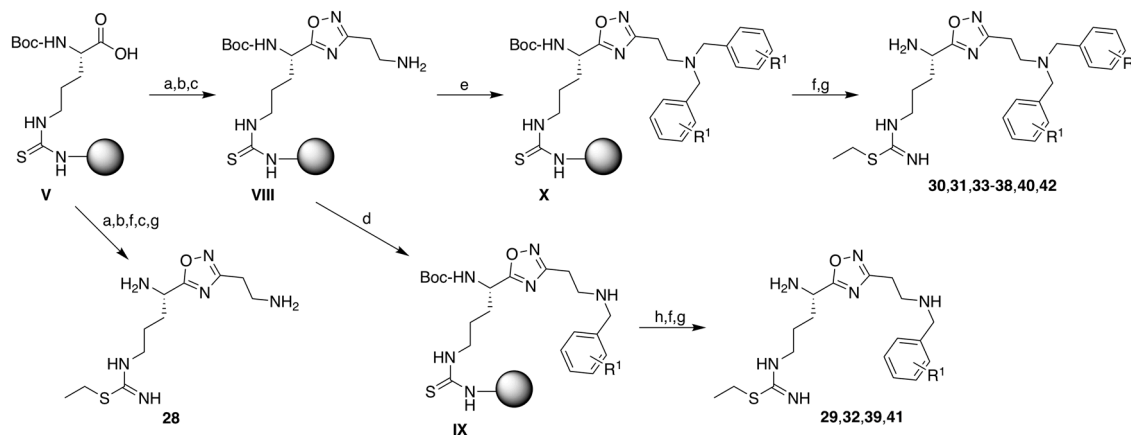
2.1. Chemistry

Several intermediates were first synthesized as described in Scheme 1. For the dipeptide-like series, the two stereoisomers of 3-amino-1-Fmoc-piperidine **3** and **4** were prepared from the corresponding 3-(Boc-amino)-piperidines by Fmoc protection in the presence of Fmoc-Cl, followed by Boc removal from the resulting compounds **1** and **2** in acidic conditions (Scheme 1A). Biphenylaldehydes **5a–5d** were obtained in one step by a Suzuki cross-coupling reaction between *m*- and *p*-bromobenzaldehydes and the corresponding phenylboronic acids (Scheme 1B). For the 1,2,4-oxadiazole series, aloc-protected 2-aminoethyl-amidoxime **6** was prepared in two steps from 2-cyano-ethylamine by amine protection in the presence of aloc-Cl followed by treatment with aqueous hydroxylamine (Scheme 1C).

All final compounds were prepared on the solid phase from a single intermediate, a $N\alpha$ -Boc-protected thiocitrulline linked to the solid support via its thiourea group (compound **V**, Schemes 2 and 3). The solid-supported intermediate **V** was synthesized as previously reported [48,49] (Scheme S1).

2.1.2. Synthesis of 1,2,4-Oxadiazole Analogs 28–42 (Scheme 3)

Compared to dipeptide-like compounds, the replacement of the amide bond by the isosteric 1,2,4-oxadiazole ring might modulate affinity, selectivity, metabolic stability, and bioavailability [52].



Scheme 3. Synthesis of monosubstituted and homo-disubstituted 1,2,4-oxadiazole analogs 28–42. Reagents and conditions: (a) amidoxime **6** (1.3 equiv.), HOBT, DIC, NMP, rt, 4 h; (b) AcONa (1.2 equiv.), THF/water (7/3), reflux, overnight (steps a and b were repeated one more time); (c) Pd(PPh₃)₄ (0.2 equiv.), PhSiH₃ (24 equiv.), DCM, rt, 4 h (twice); (d) benzaldehyde compound (3 equiv.), NaBH₄ (1.5 equiv.), DMF/MeOH (95:5), 0 °C, 15 min, + rt, 15 h; (e) benzaldehyde compound (3 equiv.), NaBH₃CN (1 equiv.), DMF/AcOH (95:5), rt, overnight; (f) 0.2 M EtI in DMF, 50 °C, 3 × 1 h; (g) TFA/TIS/H₂O (95:2.5:2.5), 40 °C, 2 × 2 h; (h) (Boc)₂O (3 equiv.), TEA (3 equiv.), DMF, 2 × 2 h.

The solid-supported intermediate **V** was coupled to amidoxime **6** (3-(*N*-allyloxycarbonyl-amino)-*N*-hydroxy-propanimidamide, Scheme 1C) using DIC/HOBt as coupling agents. The resulting compound was then cyclodehydrated in a mixture of THF/water at 80 °C and in the presence of sodium acetate, as previously described [48], followed by aloc removal with tetrakis (triphenylphosphine) palladium (0) in the presence of phenylsilane to yield the free supported primary amine **VIII**. Resin **VIII** was then treated following two sets of reductive amination conditions. Reaction with various benzaldehydes using NaBH₄ led to supported monoalkylated derivatives **IX**. To obtain complete and only single substitution, aldehydes (3 equiv.) were first incubated with the resin for 3–4 h, followed by the addition of the reducing agent (1.5 equiv.) solubilized in methanol. The reaction time should not exceed 10 h as longer times led to lower yields, maybe because of damage caused to the resin. Using NaBH₃CN led to the supported homo-dialkylated supported derivatives **X**. The best conditions included pre-incubation of benzaldehydes (3 equiv.) for 30 min in a mixture of 5% AcOH in DMF, followed by the addition of 1 equiv. reducing agent. *S*-Ethylation and TFA cleavage gave the final compounds **29–42**. In the case of monosubstituted compounds, the secondary amine of **IX** resins was first protected by treatment with Boc₂O to prevent its ethylation. Compound **28** was similarly prepared from resin **V** but *S*-ethylation was performed before aloc deprotection.

In general, the completion of each reaction was checked by an LC-MS analysis of the residue obtained after the cleavage of a small portion of the resin. The linkage between the *S*-ethylisothiourea group and the Rink amide support is quite resistant, requiring a twice-repeated prolonged TFA treatment and light warming to recover the compounds from the solid support. All compounds were obtained in low-to-medium yields (5–50%) after reverse-phase HPLC purification.

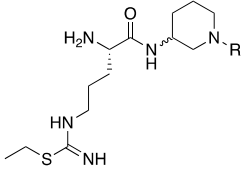
2.2. Biological Evaluation

2.2.1. Inhibition of NO Synthases

The inhibitory effects of all compounds against the three recombinant NOSs (rat nNOS, mouse iNOS, and bovine eNOS) were evaluated in 96-well plates using the oxyhemoglobin test [53]. A first screening at 100 and 10 μM was performed, and the IC_{50} values were measured for compounds showing more than 50% inhibition at 100 μM (Tables 1 and 2).

In the dipeptide-like series (Table 1), eighteen different benzyl groups have been introduced on an (*S*)-amino-piperidine moiety, and three of them have also been combined with the (*R*) isomer to check the importance of piperidine relative orientation.

Table 1. Structures of dipeptide-like compounds 7–27 and in vitro NOS inhibition (IC_{50} in μM)¹.



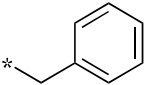
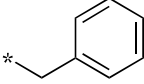
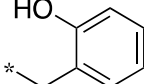
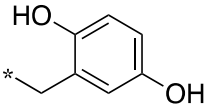
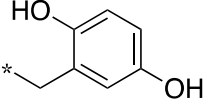
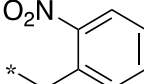
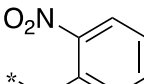
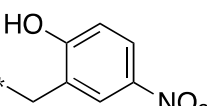
Cpds	R	St ²	IC_{50} (μM)		
			nNOS (Rat)	iNOS (Mouse)	eNOS (Bovine)
7		(S)	17.5	73.4	NI
8		(R)	15.6	25.6	NI
9		(S)	51.1	51.0	NI
10		(S)	2.0	23.9	26.7
11		(R)	17.5	73.4	25.4
12		(S)	NI	46.0	NI
13		(R)	30.6	78.9	NI
14		(S)	5.4	27.8	ND

Table 1. Cont.

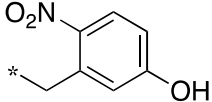
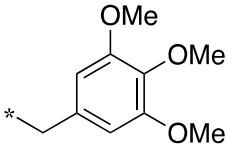
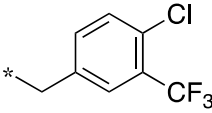
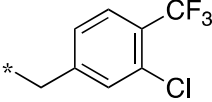
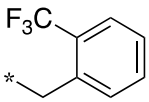
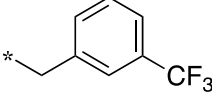
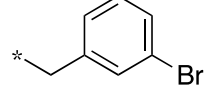
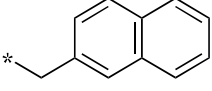
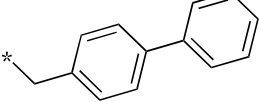
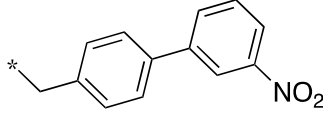
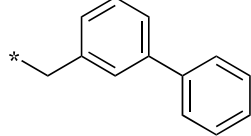
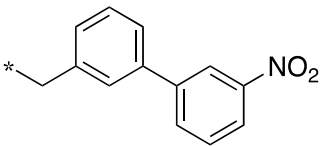
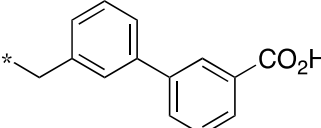
Cpds	R	St ²	IC ₅₀ (μM)		
			nNOS (Rat)	iNOS (Mouse)	eNOS (Bovine)
15		(S)	25.2	31.3	NI
16		(S)	49.6	54.9	NI
17		(S)	5.0	12.9	NI
18		(S)	6.0	NI	NI
19		(S)	7.7	NI	NI
20		(S)	15.4	NI	NI
21		(S)	1.0	45.5	NI
22		(S)	12.7	11.9	NI
23		(S)	5.4	46.9	NI
24		(S)	3.5	21.6	18.0
25		(S)	2.8	36.5	NI

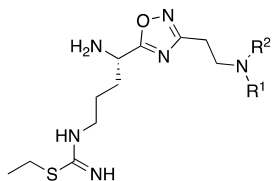
Table 1. Cont.

Cpds	R	St ²	IC ₅₀ (μM)		
			nNOS (Rat)	iNOS (Mouse)	eNOS (Bovine)
26		(S)	1.3	48.3	NI
27		(S)	9.5	NI	NI

¹ NI = no significant inhibition (<50% at 100 μM); ND = not determined. ² Stereochemistry of piperidine C³. Assays were performed in triplicate.

As observed in the previous series [48], most compounds did not inhibit eNOS and were generally not or only modest inhibitors of iNOS. In the case of nNOS, the presence of hydroxy and/or nitro or methoxy groups on the benzyl moiety was generally not favorable (9–13, 15, 16). In addition, these compounds often showed no selectivity against iNOS, and sometimes, eNOS (i.e., the two isomers, 10 and 11). One exception was compound 14, showing an IC₅₀ value in the micromolar range. In contrast, the substitution by halogens and halogenated groups (17–21) generally afforded more interesting compounds. Indeed, 17–19 and 21 were micromolar nNOS inhibitors, inactive against eNOS, and three of them (18, 19, 21) showed no or modest activity against iNOS. The introduction of a biaryl group (naphth-2-yl for compound 22, *p*- or *m*-biphenyls for 23–27) was somewhat less favorable, although most compounds displayed IC₅₀ values in the low micromolar range. Indeed, lower selectivity against iNOS was observed, and the *m*-nitro-biphenyl 24 significantly inhibited eNOS. Finally, the stereochemistry of the amino-piperidine moiety did not show a significant effect on the inhibition profile (8 vs. 7, 11 vs. 10, 13 vs. 12). This is in contrast to the result reported with similar but unsubstituted amino-piperidine-containing compounds, for which a significant difference in nNOS inhibition was observed in favor of the R isomer [51].

In the 1,2,4-oxadiazole series (Table 2), four mono- and ten disubstituted compounds have been synthesized. For comparison, the non-substituted amino compound 28 was also prepared. The latter only poorly inhibited nNOS and iNOS and was inactive against eNOS. The mono- or disubstitution of the primary amine generally led to more potent compounds (up to 200 more for 37 in the case of nNOS inhibition). It is the case of the simplest analogs bearing one or two benzyl groups (29 and 30, respectively) that significantly inhibited both NOSs with the exception of eNOS for 30. Concerning other mono/di pairs, disubstituted analogs were generally better inhibitors of nNOS and/or iNOS than their monosubstituted counterparts (i.e., 30 vs. 29 and 42 vs. 41 for both enzymes, 33 vs. 32 for nNOS only, and 40 vs. 39 for iNOS only). In the case of eNOS, the disubstitution was generally detrimental to its inhibition. One exception was compound 38, which inhibited the enzyme with an IC₅₀ value in the micromolar range.

Table 2. Structures of mono- and disubstituted 1,2,4-oxadiazoles analogs **28–42** and in vitro NOS inhibition (IC_{50} in μM)¹.


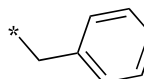
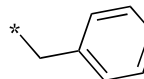
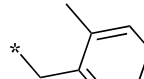
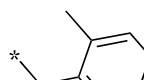
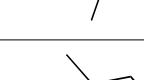
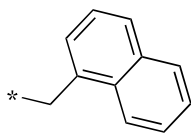
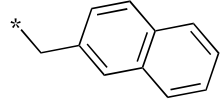
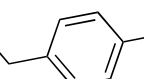
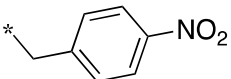
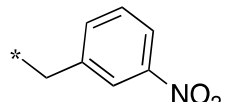
Cpds	R ¹	R ²	IC ₅₀ (μM)		
			nNOS (Rat)	iNOS (Mouse)	eNOS (Bovine)
28	-H	-H	58.9	83.7	NI
29		-H	13.4	11.1	17.9
30		-R ¹	1.6	1.3	99.6
31		-R ¹	9.9	11.1	NI
32		-H	60.1	51.6	ND
33		-R ¹	10.1	71.5	NI
34		-R ¹	1.4	4.0	NI
35		-R ¹	0.4	11.7	NI
36		-R ¹	3.1	24.3	20.2
37		-R ¹	0.3	15.8	11.8
38		-R ¹	0.6	15.9	3.9

Table 2. Cont.

Cpds	R ¹	R ²	IC ₅₀ (μM)		
			nNOS (Rat)	iNOS (Mouse)	eNOS (Bovine)
39		-H	27.0	8.0	48.2
40		-R ¹	61.0	2.0	NI
41		-H	3.0	36.3	ND
42		-R ¹	1.1	7.0	NI

¹ NI = no significant inhibition (<50% at 100 μM); ND = not determined. Assays were performed in triplicate.

Overall, as observed in the dipeptide-like series, the highest inhibitory potencies were obtained against nNOS. Indeed, several compounds displayed IC₅₀ values in the low micromolar (30, 34, 36, 41, 42) to submicromolar (35, 37, 38) range. These compounds were all disubstituted analogs (except 41) and possessed either an unsubstituted phenyl (30) or naphthyl group (34, 35) or a nitro group at any position on a phenyl ring (37, 38, 41, 42), suggesting the importance of hydrophobic interactions and/or hydrogen bonding. Therefore, a few compounds were better nNOS inhibitors than any analog in the dipeptide-like series. Unfortunately, they generally showed lower selectivity toward iNOS and/or eNOS. Anyway, the best compounds, 35 and 37, showed approximately 30- and 50-fold and >250- and 40-fold selectivity against iNOS and eNOS, respectively.

One exception was the mono/di pair 39 and 40 (*o*-nitrophenyl), which better inhibited iNOS. In particular, the disubstituted 40 showed a 30- and >50-fold selectivity toward nNOS and eNOS, respectively. This result suggested that introducing diverse bulky substituents susceptible to interaction with the substrate access channel might indeed modulate the inhibitory potency as well as the selectivity.

2.2.2. Spectral Studies

We performed UV–visible difference spectroscopy to analyze the interaction mode of some inhibitors with the heme-active site of NOS [54]. We have studied the effects of dipeptide-like compounds 7, 17, 19, 23, and 27 and 1,2,4-oxadiazole 35 on the UV–visible spectra of the oxygenase domain of nNOS (nNOS_{oxy}) and iNOS (iNOS_{oxy}) [54]. As expected [48], when added stepwise to n- and iNOS_{oxy}, all selected compounds elicited different spectra with a trough at ~425 nm and a peak at ~395 nm, similar to the substrate *L*-arginine. This profile is characteristic of type I interactions, meaning that they are bound in close proximity to the heme prosthetic group and shifted the spin state equilibrium to the pentacoordinated heme–Fe^{III} state. Double reverse plotting of the differences in absorbance between the peak at ~395 nm and valley at ~425 nm ($\Delta A_{395-425\text{ nm}}$) as a function of the concentration of the added compounds allowed calculating apparent binding constants (K_s)

(Table 3). The reference inhibitor SEITU [55] tightly bound both NOS isoforms with high affinity but no selectivity. With the exception of the dipeptide-like **27** and the heterocyclic analog **35**, which similarly interacted with both proteins, other compounds preferentially bound nNOS_{oxy} over iNOS_{oxy} with apparent affinities close to SEITU for this isoform. Interestingly, in this series of compounds, similar selectivity of nNOS over iNOS was observed when comparing inhibitory potencies, except compounds **27** and **35**, which showed significant selectivity toward nNOS (Tables 1 and 2).

Table 3. Apparent equilibrium constants (K_s , μM) for the binding of some dipeptide-like analogs **7**, **17**, **19**, **23**, and **27**, and 1,2,4-oxadiazole **35** to nNOS_{oxy} and iNOS_{oxy}¹.

Cpds	K_s (μM)	
	nNOS _{oxy}	iNOS _{oxy}
SEITU	6.4 ± 1.5	1.7 ± 0.1
7	7.1 ± 2.6	406 ± 97
17	3.6 ± 1.5	36.4 ± 4.6
19	5.2 ± 1.1	96 ± 36
23	11.4 ± 3.8	92.5 ± 8.8
27	70.6 ± 22.8	57.9 ± 8.0
35	47.1 ± 13.0	42.4 ± 8.7

¹ Titrations were performed by UV/Vis difference spectroscopy, as described in Experimental Section. Values ± SD from three different experiments. SEITU was added for comparison.

2.2.3. Cell Toxicity

Cell viability was evaluated in the murine macrophage RAW 264.7 cells using an MTT assay for compounds **18**, **21**, **26**, and **30**. This experiment was performed without or with LPS (1 $\mu\text{g}/\text{mL}$), which induces iNOS expression (Figure S1). In the absence of LPS, compounds **21** and **30** did not modify cell viability up to 100 μM , but compounds **18** and **26** were fully toxic at this concentration (Figure S1). Compound **30** only killed 20% of the cells at 500 μM (Figure S1A). In the presence of LPS (1 $\mu\text{g}/\text{mL}$), cell viability was reduced by 30% due to the inhibition by NO of key enzymes involved in cell metabolism [56] (Figure S1B). Compounds **18**, **21**, and **26** showed similar behavior as observed without LPS, but none partially reversed the LPS effect in contrast to L-NIL, SEITU, and a few of our previously reported compounds [48].

2.2.4. Inhibition of NOS in Cells

To study the potential usefulness of these compounds to inhibit NOS expressed in cells, we performed several series of experiments on selected compounds.

We evaluated the ability of selected compounds (dipeptides **7**, **8**, and **21** and 1,2,4-oxadiazoles **30** and **40**) to inhibit iNOS in RAW 264.7 cells (Figure 2), where iNOS was induced by LPS (1 $\mu\text{g}/\text{mL}$). iNOS activity was measured following LPS induction by quantifying nitrite accumulation in the supernatant. Overall, dipeptide-like compounds showed better intracellular inhibition of NO production (up to 80% inhibition at 100 μM for **21**) than oxadiazoles, despite the latter being about 20- to 30-fold more potent iNOS inhibitors. This result suggests that the 1,2,4-oxadiazole compounds were less prone to enter cells than the dipeptide-like analogs. A similar result was previously reported [48].

Finally, as some compounds are found to be more selective for nNOS rather than iNOS, we assessed the ability of dipeptide-like compounds to modulate insulin secretion in INS-1 cells in the presence of 5.6 mM glucose and in the absence of IL-1 β and, therefore, iNOS induction. Indeed, pancreatic β -cells are known to constitutively express the nNOS isoform, which negatively modulates glucose-induced insulin secretion [5]. As previously described [57], the NOS inhibitor L-NAME (5 mM) potentiated insulin release induced by 5.6 mM glucose (Figure 3). Dipeptide compounds, such as **7**, **14**, **17**, **18**, **22**, and **27** (from

500 μM to 5 mM), were also incubated for one hour to avoid potential toxic effects and were able to dose-dependently stimulate glucose insulin secretion with better efficiency than *L*-NAME. Three compounds, **13**, **21**, and **26**, displayed a maximum effect at 1 mM or 500 μM , respectively.

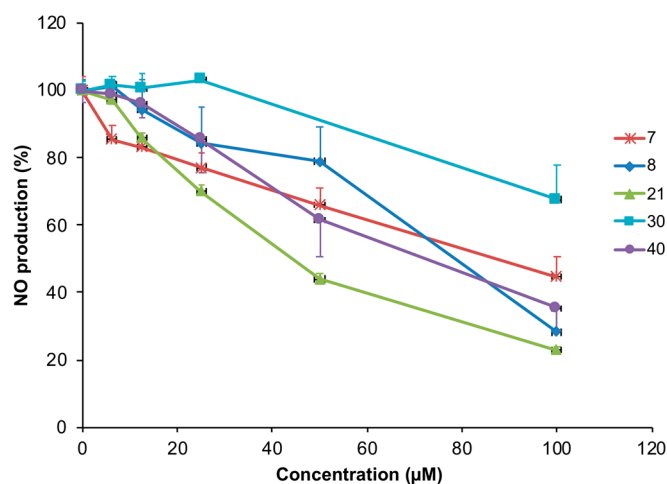


Figure 2. Inhibitory effects of dipeptides **7**, **8**, and **21** and 1,2,4-oxadiazoles **30** and **40** on NO production by RAW 264.7 cells stimulated by LPS (1 $\mu\text{g}/\text{mL}$) ($n = 3$).

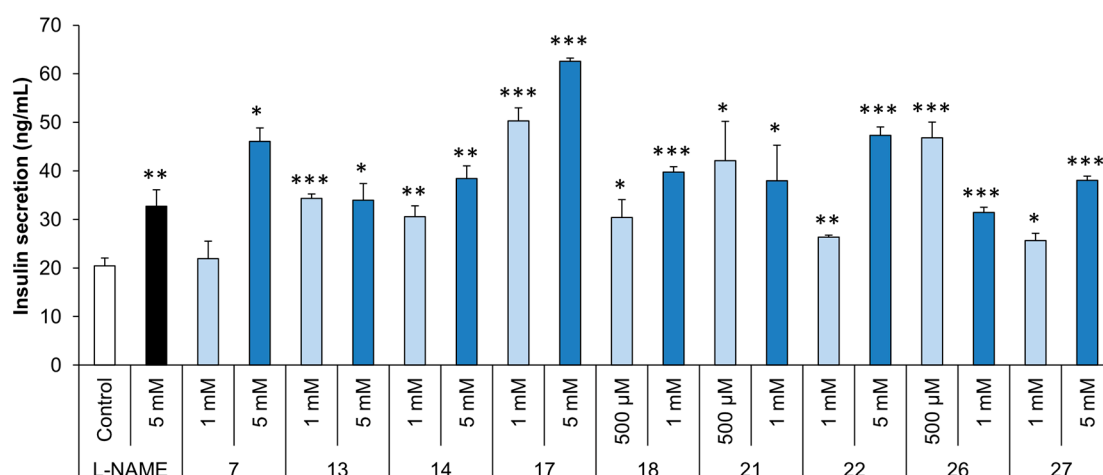


Figure 3. The effect of *L*-NAME and compounds **7**, **13**, **14**, **17**, **18**, **21**, **22**, **26**, and **27** on insulin secretion by INS-1 cells in the presence of 5.6 mM glucose and without iNOS induction with IL-1 β . Compounds were incubated simultaneously with stimulating glucose for one hour on INS-1 cells and then supernatants were collected for the measurement of insulin release. *, $p < 0.05$; **, $p < 0.01$; ***, $p < 0.001$; ($n = 3$ –5).

Overall, these results support these compounds being able to inhibit intracellular nNOS and affect cellular functions.

2.3. Modeling Study

We investigated the putative binding mode of dipeptide-like **21** and **26** and 1,2,4-oxadiazole **30** and **35** compounds within the active site of nNOS and eNOS via docking experiments. In these experiments, we assumed that the isothiourea moiety of the inhibitors will interact with the heme propionate and Glu592 and Glu363 residues in nNOS and eNOS, respectively, like the arginine guanidinium [27]. The objective was to identify potential interactions within the substrate access channel and explain the selectivity of these compounds for nNOS against eNOS.

The docking experiments were performed with AutoDock 4.2 software using the Local Search algorithm on nNOS and eNOS models generated from the crystallographic structures 1P6J and 1P6N [29], respectively, available in the Protein Data Bank (PDB). 1P6J and 1P6N are the three-dimensional structures of the complex formed between the highly selective nNOS inhibitor *L-N ω -nitroarginine-(4R)-amino-L-prolinamide* (called DP9, <https://www.rcsb.org/ligand/DP9>, accessed on 16 March 2023) and nNOS and eNOS, respectively. DP9 possesses an *N ω -nitroarginine* as a substrate analog and a 4-aminoprolinamide moiety as an extension. Our compounds were expected to similarly bind in both nNOS and eNOS. The high selectivity (i.e., 1000-fold [29]) of DP9 in favor of nNOS is mainly due to one residue variation, Asp597 in nNOS replaced by Asn368 in eNOS. In the complexes of the two isoforms with their substrate arginine (pdb codes 1OM4 and 2G6O for nNOS and eNOS, respectively), the side chain groups (protonated carboxylic for Asp597, primary amide for Asn368) make the H-bond with the α -carboxylate group of the substrate, and the H-bond network is fully identical to the two complexes. However, when introducing an extension on the α -carboxylate group of a substrate analog (as in DP9), this difference very significantly impacts the binding with eNOS [29].

We first docked the original ligand DP9 in both isoforms to check that our protocol allowed crystallographic positioning. This study was performed in the presence and absence of water molecules involved in the H-bond network formed between the enzymes and inhibitor. For each docking, only 1 cluster of 1000 solutions was obtained. As expected, while the guanidine moiety of DP9 makes a bifurcated hydrogen bonding interaction to the conserved active site glutamate in both nNOS (Glu592) and eNOS (Glu363), its α -amine establishes a strong electrostatic interaction with Glu592 in nNOS, but not Glu363 in eNOS. Compared to the crystallographic structure, an extra interaction was apparent in the docking structure between the primary amide of DP9 with one propionic acid of the heme in both isoforms. However, overall, the superimposition of the best docking pose with the crystallographic one showed very similar positioning of DP9 in both enzyme binding sites. In addition, the difference in mean docking scores was about 100-fold in favor of nNOS, in satisfactory agreement with the difference in experimental K_i values (0.1 vs. 110 μ M for nNOS and eNOS, respectively [29]).

The docking of DP9 in nNOS and eNOS was, therefore, satisfactory, and its conditions were applied to the docking of our four inhibitors. Several residues expected to be involved in binding were let flexible, including Glu592/363, Gln478/249, Arg481/252, Asn569/340, Ser477/248, and Tyr706,477 (numbering in nNOS and eNOS, respectively).

2.3.1. Compound 21

Dipeptide-like **21** is characterized by a piperidine moiety *N*-substituted by a 3-bromobenzyl group. Its docking in nNOS delivered only one pose, which corresponds to DP9 with Glu592 binding to both the isothiourea nitrogens and the α -amine (Figure 4A). However, this solution positions the bromine in a hydrophilic environment involving Arg596, Asp600, and Ser602, which is expected to be poorly favorable. Docking in eNOS yielded heterogeneous results with unfavorable mean binding energies (>-6.5 kcal/mol). The most probable pose corresponds to that observed in nNOS, and no significant difference is observed in the substrate access channel. In this case, the difference in mean binding energies (-8.3 vs. -6.5 kcal/mol for nNOS and eNOS, respectively) is probably mainly due to the difference in electrostatic energy related to the Asp597/Asn368 variation.

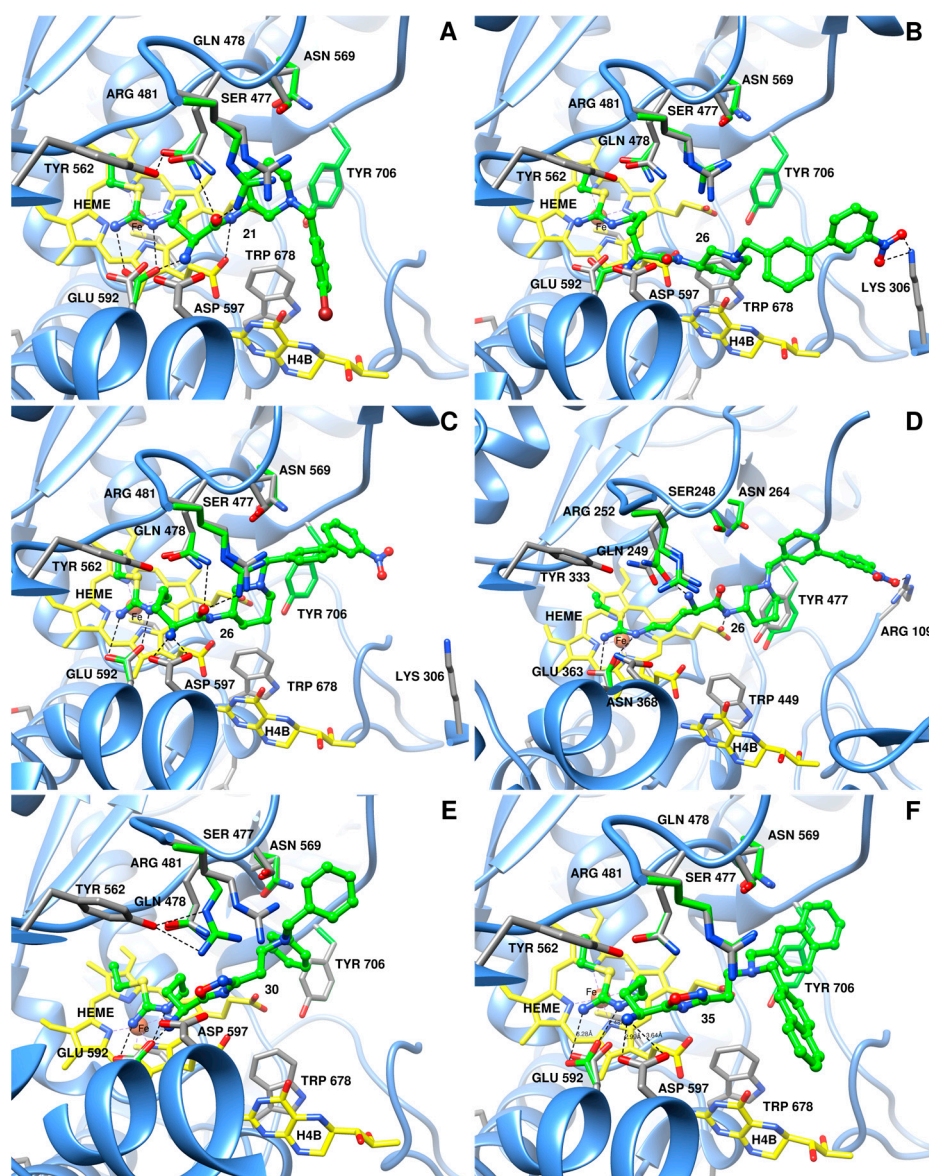


Figure 4. The best docking pose of (A) compound **21** in nNOS; (B) compound **26** in nNOS (pose 1); (C) compound **26** in nNOS (pose 2); (D) compound **26** in eNOS; (E) compound **30** in nNOS; (F) compound **35** in nNOS. Blue: protein ribbon; green stick: protein side chain adaptation in docking; green ball and stick: molecules of interest; yellow: cofactors of NOS (heme and tetrahydrobiopterin (H4B)).

2.3.2. Compound 26

The second dipeptide-like compound possesses an *m*-nitro-*m*-biphenyl substituent. In contrast to **21**, several poses were obtained when docked into nNOS. The major one shows the interaction of the α -amine with Asp597 and the nitro group with Lys304 (Figure 4B). Despite the latter interaction, the docking score is modest (a mean binding energy of -8.0 kcal/mol), possibly because it destabilizes the conserved binding between the isothiourea and Glu592. The latter is present in the second most probable pose, as well as the interaction between the α -amine and Asp597, but the nitro group is solvent-exposed and does not establish any interaction (Figure 4C).

A different pose was preferentially observed in eNOS with possible stabilizing interactions between the extending moiety of the molecule and the residues Tyr477 and Arg109 (nitro group) (Figure 4D). In this case, the positioning of the thiourea over Glu363 is not optimal, and the α -amine interacts with Gln249, which might explain why the mean

binding energies are not favorable (> -8 kcal/mol) and why the compound was found to not inhibit eNOS.

2.3.3. Compound 30

The ethylamine moiety of oxadiazole analog **30** is substituted by two benzyl groups. When docked in nNOS, the pose with the lowest binding energy corresponds to the expected one (Figure 4E). The isothiourea nitrogens and the α -amine interact with Glu592. The two benzyl groups are oriented toward Ser477 and Asn569 without performing specific interactions, and the tertiary amine is exposed to the solvent. Finally, the oxadiazole moiety does not establish any interaction. The heterocycle can only accept H-bonds, and there is no H-bond donor in its immediate environment. However, it cannot be excluded to be involved in solvent-mediated interactions.

The docking result for eNOS is identical to the result obtained with nNOS. However, a significant difference in docking score was observed in favor of nNOS (mean binding energies of -9.1 and -6.9 kcal/mol for nNOS and eNOS, respectively). It is again explained by the higher electrostatic weight for nNOS due to the Asp597/Asn368 difference between nNOS and eNOS.

2.3.4. Compound 35

Compared to **30**, the ethylamine moiety of **35** is substituted by two naphth-2-yl groups. In nNOS, the isothiourea nitrogens interact with Glu592 and the α -amine with Asp597 in most solutions. Because of their size, the naphthyls cannot stand at the same position as the benzyls of **30**. One is oriented toward Tyr706, while the second is close to Ala497. This forces the other part of the molecule to position lower in the binding site, possibly allowing the tertiary amine to interact with the propionic acid moieties of the heme group (Figure 4F). Compound **35** obtained a very good docking score (a mean binding energy of -10.2 kcal/mol) in accordance with its experimentally determined inhibitory potency (an IC_{50} value of 0.4 μ M, Table 2).

When docked in the eNOS active site, two main poses were defined. In the most populated one (a mean binding energy of -8.8 kcal/mol), the molecule shifted from the DP9-like pose where the conserved interaction with Glu363 is lost, and the α -amine makes an H-bond with Gln249. The second solution is the same for nNOS. In particular, the two naphthyls are similarly positioned. In this case, the difference in docking scores (mean binding energies of -10.2 vs. -8.4 kcal/mol for nNOS and eNOS, respectively) results again from the difference in electrostatic energies related to Asp597/Asn368 variation.

Overall, each docking showed the possibility for each molecule to interact in the substrate binding site, like DP9. However, the docking study did not show any contribution of the molecule extensions to the selectivity between nNOS and eNOS. It seems that this selectivity is only due to Asp597/Asn368 variability between the two isoforms, as shown for DP9 [29], resulting in a higher contribution of electrostatic energy to nNOS binding. The calculated mean binding energies are consistent with the experimental results, which showed that the molecules more efficiently inhibit nNOS. Whereas the extensions seemed to only marginally contribute to the binding energy, the docking experiment suggests that their size could have an impact. Compared to **21**, the docking of the more extended **26** in nNOS opens up the possibility of a favorable interaction between the nitro group and a residue in the substrate access channel, which could be achieved by the design of new molecules. In addition, the binding of oxadiazole analog **35** was found to be favorably influenced by the bulkiness of its two naphthyl groups compared to dibenzyl analog **30**. This result is consistent with the higher inhibitory potency of **35** compared to **30** (IC_{50} values of 0.4 and 1.6 μ M, respectively).

3. Conclusions

In this study, we have synthesized 36 new compounds (21 dipeptide-like compounds, 15 1,2,4-oxadiazoles) using our original solid-phase synthetic strategy.

All compounds were tested against three recombinant NOS isoforms. Overall, several new compounds showed significant inhibitory activity (an IC_{50} of about 0.3 to 15 μM) toward at least one NOS, with a global preference for nNOS that was followed by iNOS, whereas eNOS was scarcely ever inhibited. These results are in accordance with those obtained by Silverman's team on nitro-arginine-containing dipeptides and our previous studies [28]. While some dipeptide-like compounds inhibited nNOS with IC_{50} values in the micromolar range, several 1,2,4-oxadiazole analogs were submicromolar inhibitors. However, the latter were less efficient than the former in cell tests, suggesting that the 1,2,4-oxadiazole did not favor cell penetration. Finally, docking studies gave insight into the binding mode of our compounds in the substrate access channel, which will help the design of further analogs with improved activity.

4. Materials and Methods

4.1. General

4.1.1. Materials

Protected ornithine, DIC, HOBt, HBTU, DIEA, TFA, piperidine, solvents, and other reagents were purchased from Iris-Biotech, Novabiochem, Riedel-de Haën, Carlo Erba, or Acros organics and used without further purification. Fmoc Rink amide polystyrene resin (100–200 mesh, 0.94 mmol/g) was purchased from Iris-Biotech. Solvents used for RP-HPLC and LC-MS were of HPLC grade.

4.1.2. NMR Spectroscopy

^1H NMR spectra were recorded at 300, 400, or 500 MHz using $\text{DMSO-}d_6$. Splitting patterns were designated as follows: s, singlet; d, doublet; t, triplet; q, quartet; m, multiplet; and br, broad. ^{13}C NMR spectra were recorded at 75, 101, or 125 MHz using $\text{DMSO-}d_6$.

4.1.3. Analysis and Purification

RP-HPLC analysis was performed on a Chromolith SpeedRod C18 column (0.46 cm \times 5 cm) using a linear gradient (0–100%) of eluent B in A for 5 min at a flow rate of 3 mL/min.

Compounds were purified by preparative RP-HPLC on a Waters Delta Pak C18 column (40 mm \times 100 mm, 15 μm , 100 \AA) by using a linear gradient of eluent B in A at a 1%/min rate and a flow rate of 28 mL/min. Some compounds were purified on a preparative RP-HPLC coupled to a mass spectrometer (Autopurif system from Waters driven by the software MassLynx 4.0 Fractonlynx) using a Waters X Bridge Prep C18 column (19 mm \times 100 mm, 5 μm) and a linear gradient of eluent B in A (flow rate: 20 mL/min).

Eluent A: water/0.1%TFA and eluent B: acetonitrile/0.1% TFA. Detection was made at 214 nm.

Purification of precursors was performed on a column loaded with Merck silica gel 60 with a particle size of 40–63 μm .

Mass spectrometry: samples were prepared in an acetonitrile/water (50/50 *v/v*) mixture. The LC-MS system consisted of a Waters Alliance 2690 HPLC coupled to a Waters-Micromass ZQ spectrometer (electrospray ionization mode, ESI+). All separations were carried out using an RP C18 monolithic Onyx Phenomenex column (25 mm \times 4.6 mm) by means of a linear gradient (0–100%) of eluent B in A for 3 min at a flow rate of 3 mL/min. Eluent A: water/0.1% formic acid and eluent B: acetonitrile/0.1% formic acid. Positive ion electrospray mass spectra were acquired at a solvent flow rate of 100–500 $\mu\text{L}/\text{min}$. Nitrogen was used as both the nebulizing and drying gas. These data were obtained in a scan mode in 0.1 s intervals; 10 scans were summed up to obtain the final spectrum.

All final compounds were obtained as TFA salts. The HPLC retention times, calculated monoisotopic mass, measured high-resolution mass of the compounds, NMR data, and yields of purified products are reported in the Supplementary Materials.

4.2. Chemical Synthesis of the Supported Intermediates

The supported thiocitrulline intermediate **V** was prepared as reported [48] and briefly described in the Supplementary Materials (Scheme S1).

4.2.1. Synthesis of the Supported Dipeptide-like Intermediates **VI** (S) and (R)

The supported thiocitrulline intermediate **V** (1.40 mmol) was swelled in NMP for 15 min and filtered. We then successively added NMP solutions of (S) 1-*N*-Fmoc-(3-amino)-piperidine **3** (Scheme S2) (733 mg, 1.68 mmol, 1.2 equiv.), DIEA (734 μ L, 4.20 mmol, 3 equiv.), and HBTU (910 mg, 2.40 mmol, 1.5 equiv.). After 4 h of stirring, the resin was filtered and washed with DMF, methanol, and DCM. The residue obtained after a cleavage test was analyzed by LC-MS (t_R : 1.29 min; m/z (ES⁺) 496.2 (M + H⁺)).

The (R) isomer was similarly obtained from the corresponding protected 3-amino-piperidine **4**.

Fmoc removal was performed by two treatments with a 20% piperidine solution in DMF for 10 and 30 min. The resin was then washed as described above.

4.2.2. Synthesis of the Supported Dipeptide-like Intermediates **VII**: Reductive Amination

Each resin **VI** was swelled in DMF/AcOH (98/2) and a benzaldehyde (4 equiv.), including biphenyl aldehydes **5a–5d** (Scheme S3), was added. After 30 min of stirring at rt, NaBH₃CN (2 equiv.) was added, and stirring continued overnight. The resin was finally filtered and washed as described above.

4.2.3. Synthesis of the Supported 1,2,4-Oxadiazole Intermediate **VIII**

The supported thiocitrulline **V** (2.26 mmol) was placed in a balloon, swelled in NMP for 15 min, and cooled to -10 °C. We then added NMP solutions of amidoxime **6** (Scheme S4) (550 mg, 2.94 mmol, 1.3 equiv.), HOBt, H₂O (397 mg, 2.94 mmol, 1.3 equiv.), and DIC (458 μ L, 2.94 mmol, 1.3 equiv.). After 20 min at -10 °C and 4 h at room temperature, the resin was filtered and washed with DMF, methanol, and THF. For the cyclodehydration step, the resin was conditioned in THF/H₂O (7:3), an aqueous solution of sodium acetate (222 mg, 2.71 mmol, 1.2 equiv.) was added, and the mixture was refluxed for 5 h under mild stirring. After washing with DMF, methanol, and NMP, coupling and cyclodehydration were repeated.

To remove the aloc group, the resin was swelled in dry DCM, and tetrakis Pd(PPh₃)₄ (0.2 equiv.) and phenylsilane (24 equiv.) were added. The resin was stirred for 4 h and washed with DCM, methanol, and DCM. This treatment was repeated.

4.2.4. General Synthesis of the Supported 1,2,4-Oxadiazole Intermediates **IX**: Mono-Alkylation

Resin **VIII** was swelled in dry DMF and cooled to 0 °C, and a benzaldehyde compound (3 equiv.) was added. After 15 min of stirring at 0 °C and 3 h at rt, the mixture was cooled again to 0 °C, and NaBH₄ (1.5 equiv.) solubilized in a minimal volume of dry MeOH was added. After 15 min of stirring at 0 °C and 10 h at rt, the resin was filtered and washed with DMF, MeOH, and DCM.

4.2.5. General Synthesis of the Supported 1,2,4-Oxadiazole Intermediates **X**: Homo-Dialkylation

Resin **VIII** was swelled in a mixture of dry DMF/AcOH (95:5), and a benzaldehyde (3 equiv.) was added. After 30 min of stirring at rt, NaBH₃CN (1.5 equiv.) was added. The mixture was stirred overnight at rt, filtered, and washed with DMF, MeOH, and DCM.

4.2.6. Synthesis of Supported S-Ethyl-Isothiourea Derivatives

A supported thiourea derivative was swelled in DMF for 15 min and filtered and a 0.2 M solution of EtI (15 equiv.), and DMF was added. The reaction was stirred at 50 °C for 1 h and was repeated twice. The resin was then washed with DMF and DCM and dried.

4.2.7. Cleavage from the Solid Support

Deprotection and final cleavage of the compounds from the solid support were performed with TFA/TIS/H₂O (95:2.5:2.5, 10 mL/g resin) at 40 °C for 2 h. This treatment was repeated twice. After resin filtration, the filtrate was concentrated under a vacuum, and the compounds were precipitated by diethyl ether addition and recovered after centrifugation. The pellet was washed twice with a diethyl ether. When no precipitation occurred, the residues were solubilized in water/MeCN (50:50) and freeze-dried. All compounds were obtained with an average yield of 5–50% after reverse-phase HPLC purification. All compounds were above 90–95% purity.

For the cleavage test, some reaction steps (coupling, 1,2,4-oxadiazole formation, reductive amination, S-ethylation for selected compounds) were checked by cleaving 2–3 mg of resin with a solution of TFA/TIS/H₂O (95:2.5:2.5, *v/v/v*, 0.5 mL) for 1 h at room temperature. After filtration, the mixture evaporated under a nitrogen stream. The residue was solubilized in 50% MeCN/H₂O and submitted to LCMS analysis.

4.3. Biological Evaluation

L-Arginine, L-citrulline, *N*ω-nitro-L-arginine, dithiothreitol (DTT), hemoglobin, superoxide dismutase, catalase, bovine serum albumin, L-NAME, SEITU, (6*R*)-5,6,7,8-tetrahydrobiopterin, NADPH, porcine brain calmodulin, and all common salts and buffers were purchased from Sigma-Aldrich (St. Louis, MO, USA).

4.3.1. Production of Recombinant NOSs

Full-length recombinant rat nNOS, mouse iNOS, bovine eNOS, and the heme domains of rat brain nNOS and mouse iNOS were expressed in *Escherichia coli* and purified as described previously [58–62].

Protein concentrations were determined by Bradford's method using bovine serum albumin as a standard and the Bradford reagent from Biorad [63]. The heme concentrations of the purified NOS were determined optically from the [Fe^{II}-CO]–[Fe^{II}] difference spectrum using an $\Delta A_{445-480\text{ nm}}$ of 74 mM⁻¹·cm⁻¹ [64]. They were estimated to be more than 95% pure by SDS-PAGE electrophoresis.

4.3.2. Measurement of NO Production by Recombinant NOSs

NOS catalytic activity was measured using the hemoglobin capture assay [53]. The test was performed at 30 °C in 96-well microplates using a final volume of 200 μL. The assay mixture contained 100 μM NADPH, 10 μM BH₄, 6 μM HbO₂, 100 μM DTT, 5 μM FAD, 5 μM FMN, 10 μM (nNOS and eNOS), or 20 μM (iNOS) arginine, all in a 100 mM Hepes buffer, pH 7.5, and, for constitutive n- and e-NOS, 10 μg/mL calmodulin, and 1 mM CaCl₂. The studied compounds were introduced as 2 μL of ×100 concentrated solutions in DMSO, and the control experiments were performed with DMSO or the buffer only. The kinetics of NO production were measured at 401 nm using an Infinite F500 microplate reader (Tecan, Singapore).

4.3.3. Effects of Selected Compounds on UV-Visible Spectra of n- and iNOSoxy

This study was performed as previously described [48].

4.3.4. Evaluation of Cellular Models

The macrophage cell line RAW 264.7 (a gift from Dr. A. Blangy, Montpellier, France) was cultured in Dulbecco's Modified Eagle's Medium (DMEM) supplemented with 10% FCS, 100 units/mL penicillin, 100 μg/mL streptomycin, and 2 mM L-glutamine.

The insulin-secreting cell line INS-1 (a gift from Prof. C. Wolheim, Geneva, Switzerland) was cultured in RPMI-1640 supplemented with 10% FCS, 100 units/mL penicillin, 100 μg/mL streptomycin, 2 mM L-glutamine, 10 mM HEPES, 1 mM sodium pyruvate, and 50 mM 2-mercaptoethanol, according to M. Asfari et al.'s method [65].

In RAW 264.7 cells, iNOS was induced by LPS (1 µg/mL, Sigma-Aldrich) for 24 h. All studied compounds were incubated with cells during the last 24 h.

Cellular NO production was measured using the Griess reagent (Sigma-Aldrich), which evaluates the nitrite content in culture media [66]. Cellular toxicity was estimated by the MTT assay (Sigma-Aldrich) in RAW 264.7 cells after the induction (or not) of iNOS by LPS, according to the manufacturer's recommendations.

The functional effects of compounds were evaluated on INS-1 cells. Cells were preincubated for 1 h at 37 °C in a Krebs–Ringer bicarbonate buffer (108 mM NaCl, 1.19 mM KH₂PO₄, 4.74 mM KCl, 2.54 mM CaCl₂, 1.19 mM MgSO₄·7H₂O, and 18 mM NaHCO₃) containing 2 g/L BSA in the absence of glucose. After removal of the medium, the cells were stimulated for another hour at 37 °C in the same buffer in the presence of 5.6 mM glucose and the presence of increasing concentrations of *L*-NAME or compounds (from 500 µM to 5 mM). At the end of the incubation period, the medium was collected, and the insulin was measured using an insulin high-range assay kit (CisBio, Codolet, France). Data are expressed as means ± SEM of the experiments (indicated in the result part).

4.4. Modeling Study

The geometric optimization of the compound structures was performed using Gaussian 16 at the DFT level of theory with B3LYP hybrid functional and 6–31 g(d,p) basis set. The resulting structures were registered as pdb files. The molecules were then the object of charge calculation using the AM1-BCC model, and the files were registered in mol2 format using the Dockprep module found in Chimera software. Then, the docking studies were performed with AutoDock 4.2.6 [67], with Local Search as the docking algorithm and 1000 iterations. All other parameters were default values. The docking search was performed in a grid box centered on a ligand of 80 × 80 × 80 (Å³) with the standard 0.375 Å resolution to encompass all flexible side chains chosen. Files for the docking were prepared from (i) the structure of the complexes formed by *L*-*N*ω-nitroarginine-(4*R*)-amino-*L*-prolinamide (called DP9, <https://www.rcsb.org/ligand/DP9>, accessed on 16 March 2023) with nNOS (1P6J.pdb) and eNOS (1P6N.pdb) [29], which were treated as follows. Water molecules and small molecules were removed, the protein was protonated with the Dockprep module found in Chimera, charges were calculated using the AM1-BCC model, and the file was registered as the mol2 format. (ii) Compounds and protein pdbqt files were prepared with AutoDockTools (ADT) [68]. For each protein, side chains of six conserved residues were let to be flexible: Glu592/363, Gln478/249, Arg481/252, Asn569/340, Ser477/248, and Tyr706/477 (numbering for nNOS and eNOS, respectively).

Molecular graphics and analyses were performed with UCSF Chimera, developed by the Resource of Biocomputing, Visualization, and Informatics at the University of California, San Francisco, with support from NIH P41-GM103311.

Supplementary Materials: The following supporting information can be downloaded at <https://www.mdpi.com/article/10.3390/molecules28135085/s1>. Synthesis and characterization of precursors; Characterization data for dipeptides 7–27; Characterization data for 1,2,4-oxadiazole compounds 28–42; Figure S1: cell toxicity on RAW264.7 cells; Figure S2: molecular modelling (DP9); Selected ¹H and ¹³C NMR spectra; Scheme S1 (Synthesis of the supported thiocitrulline intermediate V); Scheme S2 (Synthesis of (S) and (R) 9*H*-fluoren-9-ylmethyl 3-amino-1-piperidinecarboxylate 3 and 4); Scheme S3 (Synthesis of biphenylaldehydes 5a–d); Scheme S4 (Synthesis of 3-(*N*-allyloxy-carbonyl-amino)-*N*-hydroxy-propanimidamide 6).

Author Contributions: E.M., J.C., A.E. and M.M. were involved in the compound synthesis. Biological assays were performed by J.L., K.M. and A.-D.L. Enzyme production and spectral studies were performed by B.R. and J.-L.B. Molecular modeling was performed by L.N. J.-F.H., A.-D.L. and J.-L.B. designed the study, analyzed data, and wrote the paper. J.-F.H. and A.-D.L. were involved in funding acquisition. All authors have read and agreed to the published version of the manuscript.

Funding: Part of this work was supported by the Fondation pour la Recherche Médicale (DCM20121225755).

Institutional Review Board Statement: Not applicable.

Informed Consent Statement: Not applicable.

Data Availability Statement: Data are contained within the article or Supplementary Materials.

Acknowledgments: The authors thank D. J. Stuehr (the Cleveland Clinic Foundation, Cleveland, USA) for providing NOS isozyme plasmids and Pierre Sanchez (IBMM, Montpellier, France) for performing mass spectrometry analyses.

Conflicts of Interest: The authors declare no conflict of interest. The funders had no role in the design of the study; in the collection, analyses, or interpretation of data; in the writing of the manuscript; or in the decision to publish the results.

Sample Availability: Not applicable.

References

1. Brecht, D.S.; Snyder, S.H. Nitric oxide: A physiologic messenger molecule. *Annu. Rev. Biochem.* **1994**, *63*, 175–195. [[CrossRef](#)] [[PubMed](#)]
2. Vallance, P. Nitric oxide: Therapeutic opportunities. *Fundam. Clin. Pharmacol.* **2003**, *17*, 1–10. [[CrossRef](#)]
3. Alderton, W.K.; Cooper, C.E.; Knowles, R.G. Nitric oxide synthases: Structure, function and inhibition. *Biochem. J.* **2001**, *357*, 593–615. [[CrossRef](#)] [[PubMed](#)]
4. Zhou, L.; Zhu, D.-Y. Neuronal nitric oxide synthase: Structure, subcellular localization, regulation, and clinical implications. *Nitric Oxide* **2009**, *20*, 223–230. [[CrossRef](#)] [[PubMed](#)]
5. Lajoix, A.-D.; Reggio, H.; Chardès, T.; Péraldi-Roux, S.; Tribillac, F.; Roye, M.; Dietz, S.; Broca, C.; Manteghetti, M.; Ribes, G.; et al. A neuronal isoform of nitric oxide synthase expressed in pancreatic beta-cells controls insulin secretion. *Diabetes* **2001**, *50*, 1311–1323. [[CrossRef](#)]
6. Krol, M.; Kepinska, M. Human Nitric Oxide Synthase—Its functions, polymorphisms, and inhibitors in the context of inflammation, diabetes and cardiovascular diseases. *Int. J. Mol. Sci.* **2020**, *22*, 56. [[CrossRef](#)]
7. Bogdan, C. Nitric oxide synthase in innate and adaptive immunity: An update. *Trends Immunol.* **2015**, *36*, 161–178. [[CrossRef](#)]
8. Campbell, M.G.; Smith, B.C.; Potter, C.S.; Carragher, B.; Marletta, M.A. Molecular architecture of mammalian nitric oxide synthases. *Proc. Natl. Acad. Sci. USA* **2014**, *111*, E3614–E3623. [[CrossRef](#)]
9. Stuehr, D.J.; Haque, M.M. Nitric oxide synthase enzymology in the twenty years after the Nobel Prize. *Br. J. Pharmacol.* **2019**, *176*, 177–188. [[CrossRef](#)]
10. Carvalho-Filho, M.A.; Ueno, M.; Hirabara, S.M.; Seabra, A.B.; Carvalheira, J.B.; de Oliveira, M.G.; Velloso, L.A.; Curi, R.; Saad, M.J. S-Nitrosation of the insulin receptor, insulin receptor substrate 1, and protein kinase B/Akt: A novel mechanism of insulin resistance. *Diabetes* **2005**, *54*, 959–967. [[CrossRef](#)]
11. Franco, M.C.; Estévez, A.G. Tyrosine nitration as mediator of cell death. *Cell. Mol. Life Sci.* **2014**, *71*, 3939–3950. [[CrossRef](#)] [[PubMed](#)]
12. Moldogazieva, N.T.; Lutsenko, S.V.; Terentiev, A.A. Reactive oxygen and nitrogen species-induced protein modifications: Implication in carcinogenesis and anticancer therapy. *Cancer Res.* **2018**, *78*, 6040–6047. [[CrossRef](#)] [[PubMed](#)]
13. Ferrer-Sueta, G.; Campolo, N.; Trujillo, M.; Bartsaghi, S.; Carballal, S.; Romero, N.; Alvarez, B.; Radi, R. Biochemistry of peroxynitrite and protein tyrosine nitration. *Chem. Rev.* **2018**, *118*, 1338–1408. [[CrossRef](#)] [[PubMed](#)]
14. Sims, N.R.; Anderson, M.F. Mitochondrial contributions to tissue damage in stroke. *Neurochem. Int.* **2002**, *40*, 511–526. [[CrossRef](#)] [[PubMed](#)]
15. Dawson, V.L.; Dawson, T.M. Nitric oxide in neurodegeneration. *Prog. Brain Res.* **1998**, *118*, 215–229. [[CrossRef](#)]
16. Yang, Z.; Misner, B.; Ji, H.; Poulos, T.L.; Silverman, R.B.; Meyskens, F.L.; Yang, S. Targeting nitric oxide signaling with nNOS inhibitors as a novel strategy for the therapy and prevention of human melanoma. *Antioxid. Redox Signal.* **2013**, *19*, 433–447. [[CrossRef](#)]
17. Boveris, A.; Alvarez, S.; Navarro, A. The role of mitochondrial nitric oxide synthase in inflammation and septic shock. *Free Radic. Biol. Med.* **2002**, *33*, 1186–1193. [[CrossRef](#)]
18. Perreault, M.; Marette, A. Targeted disruption of inducible nitric oxide synthase protects against obesity-linked insulin resistance in muscle. *Nat. Med.* **2001**, *7*, 1138–1143. [[CrossRef](#)]
19. Mocellin, S.; Bronte, V.; Nitti, D. Nitric oxide, a double-edged sword in cancer biology: Searching for therapeutic opportunities. *Med. Res. Rev.* **2007**, *27*, 317–352. [[CrossRef](#)]
20. Grimm, E.A.; Ellerhorst, J.; Tang, C.H.; Ekmekcioglu, S. Constitutive intracellular production of iNOS and NO in human melanoma: Possible role in regulation of growth and resistance to apoptosis. *Nitric Oxide* **2008**, *19*, 133–137. [[CrossRef](#)]
21. Li, J.; Vause, C.V.; Durham, P.L. Calcitonin gene-related stimulation of nitric oxide synthesis and release from trigeminal ganglion glial cells. *Brain Res.* **2008**, *1196*, 22–32. [[CrossRef](#)]
22. Cinelli, M.A.; Do, H.T.; Miley, G.P.; Silverman, R.B. Inducible nitric oxide synthase: Regulation, structure, and inhibition. *Med. Res. Rev.* **2020**, *40*, 158–189. [[CrossRef](#)]
23. Vallance, P.; Leiper, J. Blocking NO synthesis: How, where and why? *Nat. Rev. Drugs Discov.* **2002**, *1*, 939–950. [[CrossRef](#)] [[PubMed](#)]

24. Crane, B.R.; Arvai, A.S.; Ghosh, D.K.; Wu, C.; Getzoff, E.D.; Stuehr, D.J.; Tainer, J.A. Structure of nitric oxide synthase oxygenase dimer with pterin and substrate. *Science* **1998**, *279*, 2121–2126. [[CrossRef](#)]
25. Fischmann, T.O.; Hruza, A.; Niu, X.D.; Fossetta, J.D.; Lunn, C.A.; Dolphin, E.; Prongay, A.J.; Reichert, P.; Lundell, D.J.; Narula, S.K.; et al. Structural characterization of nitric oxide synthase isoforms reveals striking active-site conservation. *Nat. Struct. Biol.* **1999**, *6*, 233–242. [[CrossRef](#)] [[PubMed](#)]
26. Doukov, T.; Li, H.; Soltis, M.; Poulos, T.L. Single crystal structure and absorption spectral characterizations of nitric oxide synthase complexed with *N* ω -hydroxy-L-arginine and diatomic ligands. *Biochemistry* **2009**, *48*, 10246–10254. [[CrossRef](#)] [[PubMed](#)]
27. Li, H.; Jamal, J.; Plaza, C.; Pineda, S.H.; Chreifi, G.; Jing, Q.; Cinelli, M.A.; Silverman, R.B.; Poulos, T.L. Structures of human constitutive nitric oxide synthases. *Acta Cryst. D Biol. Cryst.* **2014**, *D70*, 2667–2674. [[CrossRef](#)]
28. Silverman, R.B. Design of selective neuronal nitric oxide synthase inhibitors for the prevention and treatment of neurodegenerative diseases. *Acc. Chem. Res.* **2009**, *42*, 439–451. [[CrossRef](#)]
29. Flinspach, M.L.; Li, H.; Jamal, J.; Yang, W.; Huang, H.; Hah, J.M.; Gomez-Vidal, J.A.; Litzinger, E.A.; Silverman, R.B.; Poulos, T.L. Structural basis for dipeptide amide isoform-selective inhibition of neuronal nitric oxide synthase. *Nat. Struct. Mol. Biol.* **2004**, *11*, 54–59. [[CrossRef](#)]
30. Poulos, T.L.; Li, H. Nitric oxide synthase and structure-based inhibitor design. *Nitric Oxide* **2017**, *63*, 68–77. [[CrossRef](#)]
31. Ji, H.; Stanton, B.Z.; Igarashi, J.; Li, H.; Martasek, P.; Roman, L.J.; Poulos, T.L.; Silverman, R.B. Minimal pharmacophoric elements and fragment hopping, an approach directed at molecular diversity and isozyme selectivity. Design of selective neuronal nitric oxide synthase inhibitors. *J. Am. Chem. Soc.* **2008**, *130*, 3900–3914. [[CrossRef](#)]
32. Garvey, E.P.; Oplinger, J.A.; Furfine, E.S.; Kiff, R.J.; Laszlo, F.; Whittle, B.J.; Knowles, R.G. 1400W is a slow, tight binding, and highly selective inhibitor of inducible nitric oxide synthase in vitro and in vivo. *J. Biol. Chem.* **1997**, *272*, 4959–4963. [[CrossRef](#)]
33. Zhu, Y.; Nikolic, D.; Van Breemen, R.B.; Silverman, R.B. Mechanism of inactivation of inducible nitric oxide synthase by amidines. Irreversible enzyme inactivation without inactivator modification. *J. Am. Chem. Soc.* **2005**, *127*, 858–868. [[CrossRef](#)] [[PubMed](#)]
34. Alderton, W.K.; Angell, A.D.; Craig, C.; Dawson, J.; Garvey, E.; Moncada, S.; Monkhouse, J.; Rees, D.; Russell, L.J.; Russell, R.J.; et al. GW274150 and GW273629 are potent and highly selective inhibitors of inducible nitric oxide synthase in vitro and in vivo. *Br. J. Pharmacol.* **2005**, *145*, 301–312. [[CrossRef](#)] [[PubMed](#)]
35. McMillan, K.; Adler, M.; Auld, D.S.; Baldwin, J.J.; Blasko, E.; Browne, L.J.; Chelsky, D.; Davey, D.; Dolle, R.E.; Eagen, K.A.; et al. Allosteric inhibitors of inducible nitric oxide synthase dimerization discovered via combinatorial chemistry. *Proc. Natl. Acad. Sci. USA* **2000**, *97*, 1506–1511. [[CrossRef](#)] [[PubMed](#)]
36. Nagpal, L.; Haque, M.H.; Saha, A.; Mukherjee, N.; Ghosh, A.; Ranu, B.C.; Stuehr, D.J.; Panda, K. Mechanism of inducible nitric-oxide synthase dimerization inhibition by novel pyrimidine imidazoles. *J. Biol. Chem.* **2013**, *288*, 19685–19697. [[CrossRef](#)]
37. Garcin, E.D.; Arvai, A.S.; Rosenfeld, R.J.; Kroeger, M.D.; Crane, B.R.; Andersson, G.; Andrews, G.; Hamley, P.J.; Mallinder, P.R.; Nicholls, D.J.; et al. Anchored plasticity opens door for selective inhibitor design in nitric oxide synthase. *Nat. Chem. Biol.* **2008**, *4*, 700–707. [[CrossRef](#)]
38. Van der Schueren, B.J.; Lunnon, M.W.; Laurijssens, B.E.; Guillard, F.; Palmer, J.; Van Hecken, A.; Depré, M.; Vanmolkot, F.H.; de Hoon, J.N. Does the unfavourable pharmacokinetic and pharmacodynamic profile of the iNOS inhibitor GW273629 lead to inefficacy in acute migraine? *J. Clin. Pharmacol.* **2009**, *49*, 281–290. [[CrossRef](#)]
39. Hougaard, A.; Hauge, A.W.; Guo, S.; Tfelt-Hansen, P. The nitric oxide synthase inhibitor and serotonin-receptor agonist NXN-188 during the aura phase of migraine with aura: A randomized, double-blind, placebo-controlled cross-over study. *Scand. J. Pain* **2013**, *4*, 48–52. [[CrossRef](#)]
40. Barbanti, P.; Egeo, G.; Aurilia, C.; Fofi, L.; Della-Morte, D. Drugs targeting nitric oxide synthase for migraine treatment. *Expert Opin. Investig. Drugs* **2014**, *23*, 1141–1148. [[CrossRef](#)]
41. Grover, R.; Zaccardelli, D.; Colice, G.; Guntupalli, K.; Watson, D.; Vincent, J.L. An open-label dose escalation study of the nitric oxide synthase inhibitor, *N*(G)-methyl-L-arginine hydrochloride (546C88), in patients with septic shock. Glaxo Wellcome International Septic Shock Study Group. *Crit. Care Med.* **1999**, *27*, 913–922. [[CrossRef](#)]
42. Dao, V.T.; Elbatreek, M.H.; Fuchß, T.; Grädler, U.; Schmidt, H.H.H.W.; Shah, A.M.; Wallace, A.; Knowles, R. Nitric Oxide Synthase inhibitors into the clinic at last. *Handb. Exp. Pharmacol.* **2021**, *264*, 169–204. [[CrossRef](#)]
43. Casas, A.I.; Hassan, A.A.; Larsen, S.J.; Gomez-Rangel, V.; Elbatreek, M.; Kleikers, P.W.M.; Guney, E.; Egea, J.; López, M.G.; Baumbach, J.; et al. From single drug targets to synergistic network pharmacology in ischemic stroke. *Proc. Natl. Acad. Sci. USA* **2019**, *116*, 7129–7136. [[CrossRef](#)] [[PubMed](#)]
44. Mohamed, M.F.; Marzouk, A.A.; Nafady, A.; El-Gamal, D.A.; Allam, R.M.; Abuo-Rahma, G.E.A.; El Subbagh, H.I.; Moustafa, A.H. Design, synthesis and molecular modeling of novel aryl carboximidamides and 3-aryl-1,2,4-oxadiazoles derived from indomethacin as potent anti-inflammatory iNOS/PGE2 inhibitors. *Bioorg. Chem.* **2020**, *105*, 104439. [[CrossRef](#)] [[PubMed](#)]
45. Chung, A.W.; Anand, K.; Anselme, A.C.; Chan, A.A.; Gupta, N.; Venta, L.A.; Schwartz, M.R.; Qian, W.; Xu, Y.; Zhang, L.; et al. A phase 1/2 clinical trial of the nitric oxide synthase inhibitor L-NMMA and taxane for treating chemoresistant triple-negative breast cancer. *Sci. Transl. Med.* **2021**, *13*, eabj5070. [[CrossRef](#)] [[PubMed](#)]
46. Do, H.T.; Li, H.; Chreifi, G.; Poulos, T.L.; Silverman, R.B. Optimization of blood-brain barrier permeability with potent and selective human neuronal nitric oxide synthase inhibitors having a 2-aminopyridine scaffold. *J. Med. Chem.* **2019**, *62*, 2690–2707. [[CrossRef](#)] [[PubMed](#)]

47. Vasu, D.; Li, H.; Hardy, C.D.; Poulos, T.L.; Silverman, R.B. 2-Aminopyridines with a shortened amino sidechain as potent, selective, and highly permeable human neuronal nitric oxide synthase inhibitors. *Bioorg. Med. Chem.* **2022**, *69*, 116878. [[CrossRef](#)] [[PubMed](#)]
48. Touati-Jallabe, Y.; Tintillier, T.; Mauchauffée, E.; Boucher, J.-L.; Leroy, J.; Ramassamy, B.; Hamzé, A.; Mezghenna, K.; Bouzekrini, A.; Verna, C.; et al. Solid-Phase Synthesis of substrate-based dipeptides and heterocyclic pseudo-dipeptides as potential NO Synthase inhibitors. *ChemMedChem* **2020**, *15*, 517–531. [[CrossRef](#)]
49. Hamzé, A.; Martinez, J.; Hernandez, J.-F. Solid-phase synthesis of arginine-containing peptides and fluorogenic substrates using a side-chain anchoring approach. *J. Org. Chem.* **2004**, *69*, 8394–8402. [[CrossRef](#)]
50. Huang, H.; Martasek, P.; Roman, L.J.; Silverman, R.B. Synthesis and evaluation of peptidomimetics as selective inhibitors and active site probes of nitric oxide synthases. *J. Med. Chem.* **2000**, *43*, 2938–2945. [[CrossRef](#)]
51. Seo, J.; Martásek, P.; Roman, L.J.; Silverman, R.B. Selective L-nitroargininylaminopyrrolidine and L-nitroargininylaminopiperidine neuronal nitric oxide synthase inhibitors. *Bioorg. Med. Chem.* **2007**, *15*, 1928–1938. [[CrossRef](#)]
52. Boström, J.; Hogner, A.; Llinas, A.; Wellner, E.; Plowright, A.T. Oxadiazoles in medicinal chemistry. *J. Med. Chem.* **2012**, *55*, 1817–1830. [[CrossRef](#)]
53. Hevel, J.M.; Marletta, M.A. Nitric oxide synthase assays. *Meth. Enzymol.* **1994**, *233*, 250–258. [[CrossRef](#)]
54. McMillan, K.; Masters, B.S. Optical difference spectrophotometry as a probe of rat brain nitric oxide synthase heme-substrate interaction. *Biochemistry* **1993**, *32*, 9875–9880. [[CrossRef](#)] [[PubMed](#)]
55. Nakane, M.; Klinghofer, V.; Kuk, J.E.; Donnelly, J.L.; Budzik, G.P.; Pollock, J.S.; Basha, F.; Carter, G.W. Novel potent and selective inhibitors of inducible nitric oxide synthase. *Mol. Pharmacol.* **1995**, *47*, 831–834. [[PubMed](#)]
56. Brown, G.C.; Cooper, C.E. Nanomolar concentrations of nitric oxide reversibly inhibit synaptosomal respiration by competing with oxygen at cytochrome oxidase. *FEBS Lett.* **1994**, *356*, 295–298. [[CrossRef](#)]
57. Lajoix, A.-D.; Badiou, S.; Péraldi-Roux, S.; Chardès, T.; Dietz, S.; Aknin, C.; Tribillac, F.; Petit, P.; Gross, R. Protein inhibitor of neuronal nitric oxide synthase (PIN) is a new regulator of glucose-induced insulin secretion. *Diabetes* **2006**, *55*, 3279–3288. [[CrossRef](#)]
58. Moali, C.; Boucher, J.-L.; Sari, M.A.; Stuehr, D.J.; Mansuy, D. Substrate specificity of NO synthases: Detailed comparison of L-arginine, homo-L-arginine, their N ω -hydroxy derivatives, and N ω -hydroxynor-L-arginine. *Biochemistry* **1998**, *37*, 10453–10460. [[CrossRef](#)]
59. Wu, C.; Zhang, J.; Abu-Soud, H.; Ghosh, D.K.; Stuehr, D.J. High-level expression of mouse inducible nitric oxide synthase in *Escherichia coli* requires coexpression with calmodulin. *Biochem. Biophys. Res. Commun.* **1996**, *222*, 439–444. [[CrossRef](#)] [[PubMed](#)]
60. Ghosh, S.; Gachhui, R.; Crooks, C.; Wu, C.; Lisanti, M.P.; Stuehr, D.J. Interaction between caveolin-1 and the reductase domain of endothelial nitric-oxide synthase. Consequences for catalysis. *J. Biol. Chem.* **1998**, *273*, 22267–22271. [[CrossRef](#)]
61. Abu-Soud, H.M.; Gachhui, R.; Raushel, F.M.; Stuehr, D.J. The ferrous-dioxy complex of neuronal nitric oxide synthase. Divergent effects of L-arginine and tetrahydrobiopterin on its stability. *J. Biol. Chem.* **1997**, *272*, 17349–17353. [[CrossRef](#)] [[PubMed](#)]
62. Ghosh, D.K.; Wu, C.; Pitters, E.; Moloney, M.; Werner, E.R.; Mayer, B.; Stuehr, D.J. Characterization of the inducible nitric oxide synthase oxygenase domain identifies a 49 amino acid segment required for subunit dimerization and tetrahydrobiopterin interaction. *Biochemistry* **1997**, *36*, 10609–10619. [[CrossRef](#)] [[PubMed](#)]
63. Bradford, M.M. A rapid and sensitive method for the quantitation of microgram quantities of protein utilizing the principle of protein-dye binding. *Anal. Biochem.* **1976**, *72*, 248–252. [[CrossRef](#)]
64. Stuehr, D.J.; Ikeda-Saito, M. Spectral characterization of brain and macrophage nitric oxide synthases. Cytochrome P-450-like heme proteins that contain a flavin semiquinone radical. *J. Biol. Chem.* **1992**, *267*, 20547–20550. [[CrossRef](#)] [[PubMed](#)]
65. Asfari, M.; Janjic, D.; Meda, P.; Li, G.; Halban, P.A.; Wollheim, C.B. Establishment of 2-mercaptoethanol-dependent differentiated insulin-secreting cell lines. *Endocrinology* **1992**, *130*, 167–178. [[CrossRef](#)]
66. Green, L.C.; Wagner, D.A.; Glogowski, J.; Skipper, P.L.; Wishnok, J.S.; Tannenbaum, S.R. Analysis of nitrate, nitrite, and [^{15}N]nitrate in biological fluids. *Anal. Biochem.* **1982**, *126*, 131–138. [[CrossRef](#)]
67. Morris, G.M.; Huey, R.; Lindstrom, W.; Sanner, M.F.; Belew, R.K.; Goodsell, D.S.; Olson, A.J. AutoDock4 and AutoDockTools4: Automated docking with selective receptor flexibility. *J. Comput. Chem.* **2009**, *16*, 2785–2791. [[CrossRef](#)]
68. Sanner, M.F. Python: A programming language for software integration and development. *J. Mol. Graph. Mod.* **1999**, *17*, 57–61.

Disclaimer/Publisher's Note: The statements, opinions and data contained in all publications are solely those of the individual author(s) and contributor(s) and not of MDPI and/or the editor(s). MDPI and/or the editor(s) disclaim responsibility for any injury to people or property resulting from any ideas, methods, instructions or products referred to in the content.